

Self-Powered Broadband Photodetector Based on MoS₂/Sb₂Te₃ Heterojunctions: A promising approach for highly sensitive detection

Hao Wang^{1,2}, Yaliang Gui¹, Chaobo Dong¹, Salem Altaieb¹, Behrouz Movahhed Nouri², Martin Thomaschewski¹, Hamed Dalir^{1,2}, and Volker J. Sorger^{1,2}

¹Department of Electrical and Computer Engineering, George Washington University, Washington, DC 20052, USA

²Optelligence LLC, Upper Marlboro, Maryland 20772, USA

Abstract

Topological insulators have shown great potential for future optoelectronic technology due to their extraordinary optical and electrical properties. Photodetectors, as one of the most widely used optoelectronic devices, are crucial for sensing, imaging, communication, and optical computing systems to convert optical signals to electrical signals. Here we experimentally show a novel combination of topological insulators (TIs) and transition metal chalcogenides (TMDs) based self-powered photodetectors with ultra-low dark current and high sensitivity. The photodetector formed by a MoS₂/Sb₂Te₃ heterogeneous junction exhibits a low dark current of 2.4 pA at zero bias and 1.2 nA at 1V. It shows a high photoresponsivity of > 150 mA W⁻¹ at zero bias and rectification of 3 times at an externally applied bias voltage of 1V. The excellent performance of the proposed photodetector with its innovative material combination of TMDs and TIs paves the way for the development of novel high-performance optoelectronic devices. The TIs/TMDs transfer used to form the heterojunction is simple to incorporate into on-chip waveguide systems, enabling future applications on highly integrated photonic circuits.

Introduction

Transition metal chalcogenides (TMDs) have been widely explored as active materials for high-performance optoelectronics due to their unique physical properties.¹⁻³ Transition metal chalcogenides optoelectronics usually suffer from surface oxidation, high contact resistance, and relatively low mobilities.⁴⁻⁷ To alleviate the aforementioned disadvantages of TMD-based photodetectors, recent technologies utilize plasmonic enhancement to improve the light-matter interaction of TMDs, while others use heterostructures to adjust inherent electrical and optical characteristics and graphene contact to aid charge carrier injection and extraction; those all exhibit attractive performance improvements such as higher sensitivity, broader frequency response, improved external quantum efficiencies (EQE), higher detectivity (D*) and a broader spectral photoresponse.⁴⁻⁹ However, combining topological insulators (TIs) as a novel quantum materials group with the attractive features of TMDs has remained largely unexplored. Topological insulators itself exhibit various appealing optoelectronic features¹²⁻¹⁴ which find applications in high-performance photodetection, e.g., due to its unique energy band structure. Furthermore, the topologically protected gapless conductive edge states or surface states in TIs offer extraordinarily high mobility and a broad detection spectrum compared to graphene which has zero bandgaps.¹⁵⁻¹⁹ Topological insulators are also mechanically flexible materials that can be used in wearable technology. Most TMDs are easily oxidized under atmospheric environments, whereas TIs are more stable in normal conditions. As a monolayer, molybdenum disulfide (MoS₂) has a direct bandgap of 1.8 eV, whereas, in bulk, it has an indirect bandgap of 1.3 eV.²⁰ The visible to the infrared absorption spectrum of MoS₂ ranges from 350 to 950 nm which is utilized in various optoelectronic applications such as light-harvesting, photovoltaics, and photodetection.²¹⁻²⁶ Here, we demonstrate a vertical heterojunction-based photodetector with TIs and TMDs, which provide a promising tool for manipulating the electrical and optical properties of the individual materials. The heterojunction-based photodetector, formed by MoS₂ and Sb₂Te₃ exfoliation and deterministic transfer to a silicon oxide substrate, shows reduced dark current, high responsivity $R=I_{\text{photo}}/P_{\text{laser}}$ (defined by the ratio between the photocurrent I_{photo} and the incident laser power P_{laser}), and a self-driven detection range from visible to near-infrared wavelengths. The photocarrier separation is accelerated, and photocarrier recombination is suppressed due to the inherent difference in their energy level. Compared to single TMDs, it also exhibits a reduced dark current, which is beneficial for achieving high detection sensitivities at reduced power consumption. The dark current is ~10 pA, and the light-induced on/off ratio is more than 10³ due to the interlayer built-in field and a broadband response from 500

nm to 900 nm. Besides the demonstrated free-space application, the proposed device has potential in densely integrated applications such as digital to analog converter system or photonic integrated circuits due to the ease of integration with photonic waveguide technology.²³⁻²⁶

Results and Discussion

To fabricate the device, Sb_2Te_3 and MoS_2 layers were prepared by mechanical exfoliation and transferred to a SiO_2/Si substrate by the pick and drop technique. These two layers are stacked by weak van der Waals force (Fig.1a). Three Ti/Au electrodes formed by electron beam evaporation act as the electrical contact pads to inject and extract the photocurrent generated by the photodetector. Two electrodes are placed on the top of the MoS_2 and one electrode is placed on the Sb_2Te_3 (Fig.1b). The compact total junction size is measured to be only 0.16 mm^2 . A Schottky barrier is present when the electrode is contacted with the $\text{MoS}_2/\text{Sb}_2\text{Te}_3$ layers to reach the equilibrium state, and it also generates a tunneling current. However, the applied heterostructure minimizes the depletion region due to the atomically thin layer. The photocarriers can be efficiently separated at the heterostructure interface with the built-in electric field in the PN heterojunction or an external electric field from an applied bias, yielding photocurrent across the heterostructure channel. As a result, there is no significant potential barrier in the forward direction, which increase the photodetector's responsivity (Fig.1c).

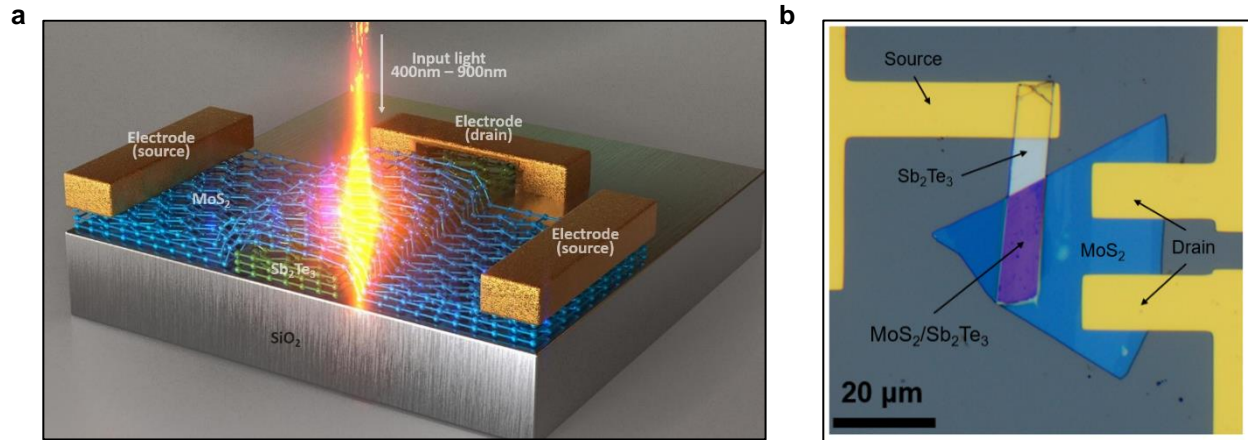


Figure 1. $\text{Sb}_2\text{Te}_3/\text{MoS}_2$ pn junction heterostructure photodetector (a) A schematic representation of the $\text{Sb}_2\text{Te}_3/\text{MoS}_2$ van der Waals p-n junction photodetector. (b) The optical microscope image of PN junction device

Raman and Energy-dispersive X-ray spectroscopy (EDS) measurements are used to characterize the spatial structure and properties of the vertically stacked $\text{MoS}_2/\text{Sb}_2\text{Te}_3$ system. Raman spectra are collected via 532 nm laser illumination. The Raman signal of MoS_2 showed two distinct peaks at 384 cm^{-1} and 409 cm^{-1} in the spectrum Fig. 2(d), which were indicated the in-plane Mo-S phonon mode (E_{2g}^1 at 384 cm^{-1}) and out of plane Mo-S phono mode (A_{1g} at 409 cm^{-1}) of MoS_2 respectively.^{30,31} Raman Spectra evidence the MoS_2 multilayer film with a stoke shift of 25 cm^{-1} .³² The Raman spectrum of Sb_2Te_3 consists of different peaks related to Sb_2Te_3 vibrations: 70 cm^{-1} , 114 cm^{-1} , 130 cm^{-1} with two peaks centered at 97 cm^{-1} , and 105 cm^{-1} between, 146 cm^{-1} , 167 cm^{-1} . The 70 cm^{-1} , 97 cm^{-1} and 167 cm^{-1} peaks indicated the A_{1g} and E_g normal modes of the Sb-Te vibrations. The 114 cm^{-1} , 105 cm^{-1} , and 146 cm^{-1} indicate the Te-Te interactions, which together consist of the whole structure of Sb_2Te_3 .³² The thickness of Sb_2Te_3 is estimated to be above 65 nm .³³ Energy Dispersive Spectroscopy (EDS) is employed to explore the element information collected from the single layers (the exfoliated MoS_2 (point C), and Sb_2Te_3 (point A) and stacked layers ($\text{MoS}_2/\text{Sb}_2\text{Te}_3$ (point B)) on the device, respectively (Fig. 2(b)). The corresponding MoS_2 EDS spectrum shows the L series peaks of Mo and S K_α peak is very pronounced; therefore, only a widened peak with a tail towards the high energy end can be seen with EDS. The elemental compositions (Sb/Te) of the exfoliated Sb_2Te_3 layers were also determined by EDS. We observed two weak X-ray emission peaks corresponded to Sb and Te. The spectrum also showed the characteristic peaks of Si, which originates from the used substrate. The absence of any other peaks indicates that the Sb_2Te_3 layers are formed from Sb and Te, only. The quantitative atomic ratio of Sb and Te is roughly 38.7% to 61.3%, which is near to the 2:3 stoichiometry ratio in accordance to the EDS investigations of Sb_2Te_3 .³⁴⁻³⁶

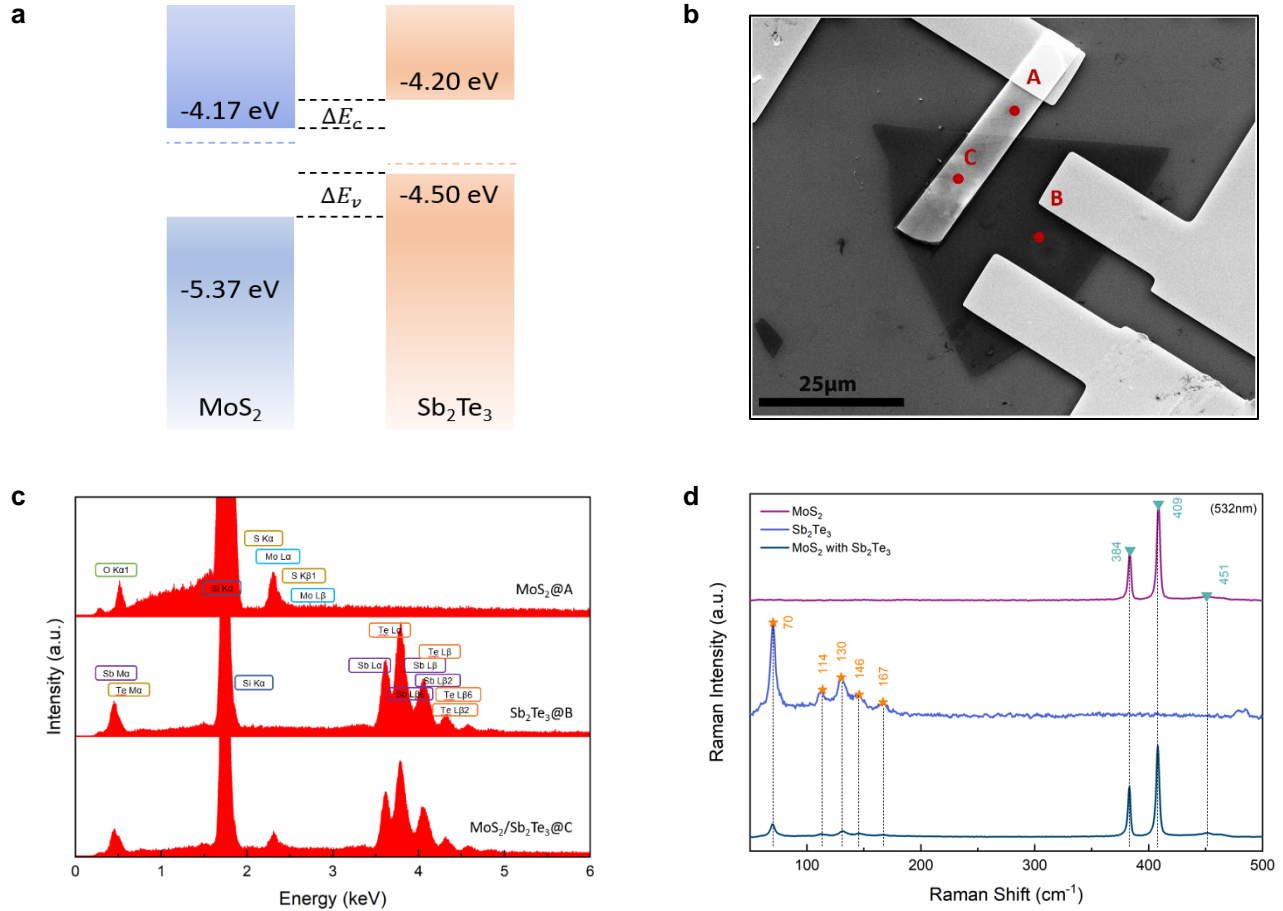


Fig. 2. Material characterization of the Sb₂Te₃/MoS₂ heterojunction (a) Band structures of the vdW layered MoS₂/Sb₂Te₃ heterojunction (b) SEM image of the fabricated device with point A on Sb₂Te₃, point B on MoS₂ and point C on the MoS₂/Sb₂Te₃ heterojunction. Two electrodes are on top of the MoS₂ layer and one on top of the Sb₂Te₃. (c) As shown in the SEM image, EDS signals were collected at three distinct positions to characterize the materials. (d) Raman spectra were collected from the pure MoS₂ and Sb₂Te₃ and the Sb₂Te₃/MoS₂ PN junction region with a 532 nm laser.

Prior to the optoelectronic measurements, we characterized the electrical performance of the MoS₂/Sb₂Te₃ junction by applying a source-drain bias voltage V_{sd} from -1 to 1 V to evaluate the dark current and performance of the van der Waals PN heterojunction. As indicated by the black curve in the I-V measurement (inset of Fig. 3a, 3b and 3c), the dark currents are stable and consistent. The dark current is as low as 2.38 pA at zero bias and 1.16 nA at 1 V bias, which benefits from the heterostructure design. To our best knowledge, this is the lowest dark current in a vdW heterojunction photodetector compared to other vdW heterojunction photodetectors.^{37–45} At a positive bias, the dark current becomes significantly higher than at negative voltages. Furthermore, under on and off bias voltage V_{sd} , the source-drain current, I_{sd} has a rectifying characteristic. This reveals that a vdW PN heterojunction is created at the interface of the stacked MoS₂/Sb₂Te₃. The diode's on/off ratio, defined as the ratio between photogenerated current and dark current, is around 5.6×10^3 . At room temperature, the ultra-low dark current and high on/off ratio at zero bias enable the development of a highly sensitive self-powered photodetector. The power dependent IV measurement of the PN heterojunction at the wavelength of 500 nm, 700 nm, and 900 nm has also been performed (inset of Fig. 3a, 3b and 3c). At zero bias voltage, the heterojunction separates the photogenerated electro-hole pairs and introduces the photocurrent due to the built-in electric field formed at the MoS₂/Sb₂Te₃ interface. The photocurrent I_{photo} increases with higher optical power illumination because electro-hole pairs generation rates increase. This demonstrates self-powered photodetection at various wavelengths (Fig. 3a, 3b and 3c with the insets in Figure 3(a)(b)(c) showing the measured I_{photo} and I_{sc} as a function of the optical power at various wavelengths. The I_{photo} increases

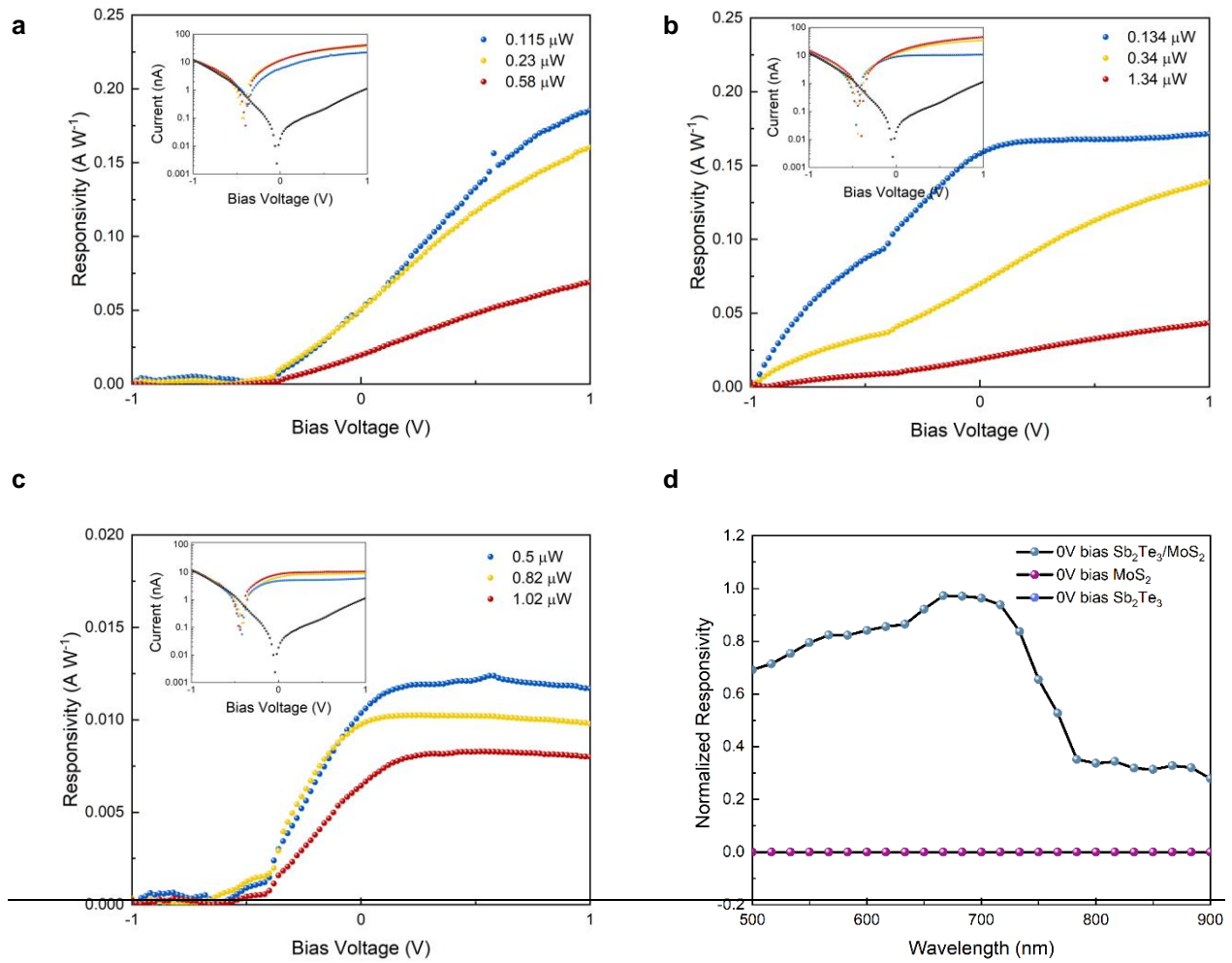


Fig. 3. Electrical characterization of $\text{Sb}_2\text{Te}_3/\text{MoS}_2$ PN junction heterostructure photodetector. (a), (b), (c) The measured photoresponsivity at different wavelengths, 500nm, 700nm, and 900nm, under -1 to 1 V bias voltage. At zero bias, the photoresponsivity was clearly observed and increased proportionally to the optical power. (d) Normalized responsivity by sweeping the wavelength under 0 bias from 500 nm to 900 nm with a step size of 10nm, which indicates a broad wavelength response.

proportionally to the illuminated optical power, which gives evidence of the photovoltaic effect in the vdW PN heterojunction. The responsivity of the $\text{Sb}_2\text{Te}_3/\text{MoS}_2$ PN junction-based heterostructure photodetector is measured from -1 V to +1 V at the wavelength of 500 nm, 700 nm, and 900 nm using the free-space optical setup. With a positive bias voltage, an external electric field is formed at the junction interface, increasing the separation efficiency of the photogenerated carriers and, therefore, the responsivity. At +1 V bias, the responsivity was amplified 1.5 to 3 times depending on the wavelength and optical power. The responsivity grows with the applied voltage and gradually saturates depending on the incident optical power. Under zero bias, the significant broadband photocurrent of the PN junction photodetector was observed within a wavelength range from 500 to 900 nm (Fig.3d). The highest responsivity under zero bias was 156 mA W^{-1} at 650 nm.

Conclusion

In conclusion, we proposed and experimentally demonstrate a self-powered, extremely sensitive photodetector based on a novel combination of a topological insulator and TMDs van der Waals PN heterojunction. Due to the current rectifying property of the PN heterojunction, the constructed device exhibits extremely low dark current and high responsivities. Under zero bias, the dark current of the device is 2.4 pA and the responsivity of 156 mA W⁻¹. By increasing the bias voltage to 1 V, the responsivity was magnified thrice due to the external field amplification. This outstanding performance of the proposed photodetector with its novel material combination paves the way for further research and applications based on other TMDs and Tis in optoelectronic applications.⁴⁶⁻⁴⁹ The PN heterojunction transfer can be easily integrated into waveguide systems, allowing for future applications in PICs. Indeed, as nano-optics becomes practical⁵⁰, efficient photodetectors augment other optoelectronic devices based on 2D materials⁵¹ such novel sources or energy-converters for renewable energy⁵².

Methods

Device fabrication

The Sb₂Te₃/MoS₂ PN junction heterostructure is formed using 2D flakes exfoliated from the bulk crystals and transferred by the pick and drop transfer system (See supplementary for more information) on Si/SiO₂ substrate. The electrical contact pads were formed using e-beam lithography (Raith Pioneer EBL) and metal thermal evaporation were employed to deposit the Ti/Au (5 nm / 50 nm) electrodes on the produced heterostructures. The lift-off was performed by acetone, then rinsing in isopropyl alcohol and nitrogen drying in RT (room temperature).

Device experimentation

The tunable (NKT SUPERCONTINUUM Compact) source and the source meter (Keithly 2600B) was used for electrical response measurements of Sb₂Te₃/MoS₂ PN junction heterostructure devices. The laser beam was focused on the devices by an objective lens. The Raman was performed using a 532 nm laser source at room temperature.

Acknowledgments

This work was performed in part at the George Washington University Nanofabrication and Imaging Center (GWNIC).

References

1. Xue, Y. *et al.* Scalable production of a Few-Layer MoS₂/WS₂ vertical heterojunction array and its application for photodetectors. *ACS Nano* **10**, 573–580 (2016).
2. Huang, Y. *et al.* Van der Waals Coupled Organic Molecules with Monolayer MoS₂ for Fast Response Photodetectors with Gate-Tunable Responsivity. *ACS Nano* **12**, 4062–4073 (2018).
3. Bie, Y. Q. *et al.* A MoTe₂-based light-emitting diode and photodetector for silicon photonic integrated circuits. *Nat. Nanotechnol.* **12**, 1124–1129 (2017).
4. Patil, C. *et al.* Self-Driven Highly Responsive PN Junction InSe Heterostructure Near-Infrared Light Detector Invited. *Photonics Res.* **10**, 97–105 (2022).
5. Maiti, R. *et al.* Loss and coupling tuning via heterogeneous integration of MoS₂ layers in silicon photonics [Invited] . *Opt. Mater. Express* **9**, 751 (2019).
6. Maiti, R. *et al.* Strain-engineered high-responsivity MoTe₂ photodetector for silicon photonic integrated circuits. *Nat. Photonics* **14**, 578–584 (2020).
7. Patil, C. *et al.* Highly accurate, reliable, and non-contaminating two-dimensional material transfer system. *Appl. Phys. Rev.* **9**, (2022).
8. Cheng, R. *et al.* Electroluminescence and photocurrent generation from atomically sharp WSe₂/MoS₂ heterojunction p-n diodes. *Nano Lett.* **14**, 5590–5597 (2014).

9. Lopez-Sanchez, O. *et al.* Light generation and harvesting in a van der waals heterostructure. *ACS Nano* **8**, 3042–3048 (2014).
10. Zhang, W. *et al.* Role of metal contacts in high-performance phototransistors based on WSe2 monolayers. *ACS Nano* **8**, 8653–8661 (2014).
11. Huang, H. *et al.* Highly sensitive visible to infrared MoTe2 photodetectors enhanced by the photogating effect. *Nanotechnology* **27**, (2016).
12. Ganeev, R. A. *et al.* Exfoliated Bi2Te3nanoparticle suspensions and films: Morphological and nonlinear optical characterization. *Nanophotonics* **10**, 3857–3870 (2021).
13. Yin, Q. *et al.* Self-powered topological insulator Bi 2 Te 3 /Ge heterojunction photodetector driven by long-lived excitons transfer . *Nanotechnology* **33**, 255502 (2022).
14. Ruan, S. *et al.* Terahertz probe of nonequilibrium carrier dynamics and ultrafast photocurrents in the topological insulator Sb2Te3. *Appl. Phys. Lett.* **118**, (2021).
15. Hasan, M. Z. & Kane, C. L. Colloquium: Topological insulators. *Rev. Mod. Phys.* **82**, 3045–3067 (2010).
16. Topological, T. *et al.* Experimental Realization of a. **178**, 1–4 (2009).
17. Fu, L., Kane, C. L. & Mele, E. J. Topological insulators in three dimensions. *Phys. Rev. Lett.* **98**, 1–4 (2007).
18. Butler, S. Z. *et al.* Progress, challenges, and opportunities in two-dimensional materials beyond graphene. *ACS Nano* **7**, 2898–2926 (2013).
19. Zhang, H. *et al.* Topological insulators in Bi 2 Se 3, Bi 2 Te 3 and Sb 2 Te 3 with a single Dirac cone on the surface. *Nat. Phys.* **5**, 438–442 (2009).
20. Rahman, I. A. & Purqon, A. First Principles Study of Molybdenum Disulfide Electronic Structure. *J. Phys. Conf. Ser.* **877**, (2017).
21. Zhang, W. *et al.* High-gain phototransistors based on a CVD MoS2 monolayer. *Adv. Mater.* **25**, 3456–3461 (2013).
22. Roy, K. *et al.* Graphene-MoS 2 hybrid structures for multifunctional photoresponsive memory devices. *Nat. Nanotechnol.* **8**, 826–830 (2013).
23. Lopez-Sanchez, O., Lembke, D., Kayci, M., Radenovic, A. & Kis, A. Ultrasensitive photodetectors based on monolayer MoS 2. *Nat. Nanotechnol.* **8**, 497–501 (2013).
24. Tsai, M. *et al.* Monolayer MoS 2 Heterojunction Solar. *ACS Nano* **8**, 8317–8322 (2014).
25. Bernardi, M., Palummo, M. & Grossman, J. C. Extraordinary sunlight absorption and one nanometer thick photovoltaics using two-dimensional monolayer materials. *Nano Lett.* **13**, 3664–3670 (2013).
26. Lou, J., Xu, X. & Ye, P. D. Black Phosphorus Monolayer MoS 2 Diode. *ACS Nano* **8**, 8292–8299 (2014).
27. Tahersima, M. H. *et al.* Coupling-enhanced dual ITO layer electro-absorption modulator in silicon photonics. *Nanophotonics* **8**, 1559–1566 (2019).
28. Gui, Y., Nouri, B. M., Miscuglio, M., Amin, R. & Wang, H. monolithic ITO Mach – Zehnder interferometer modulator enabling 3500 times higher packing density. **3334**, (2022).
29. Amin, R. *et al.* An ITO-graphene heterojunction integrated absorption modulator on Si-photonics for neuromorphic nonlinear activation. *APL Photonics* **6**, (2021).
30. Li, H., Wu, J., Yin, Z. & Zhang, H. Preparation and applications of mechanically exfoliated single-layer and multilayer MoS2 and WSe2 nanosheets. *Acc. Chem. Res.* **47**, 1067–1075 (2014).
31. Li, H. *et al.* From bulk to monolayer MoS 2: Evolution of Raman scattering. *Adv. Funct. Mater.* **22**, 1385–

- 1390 (2012).
32. Thripuranthaka, M., Kashid, R. V., Sekhar Rout, C. & Late, D. J. Temperature dependent Raman spectroscopy of chemically derived few layer MoS₂ and WS₂ nanosheets. *Appl. Phys. Lett.* **104**, (2014).
 33. Hao, G. *et al.* Spiral growth of topological insulator Sb₂Te₃ nanoplates. *Appl. Phys. Lett.* **102**, 1–5 (2013).
 34. Zhang, G. *et al.* Quintuple-layer epitaxy of thin films of topological insulator Bi₂Se₃. *Appl. Phys. Lett.* **95**, 95–98 (2009).
 35. Physics, A. Micro-Raman spectroscopy of mechanically exfoliated few-quintuple layers of Bi₂Te₃, Micro-Raman Spectroscopy of Mechanically Exfoliated Few-Quintuple Layers of Bi₂Te₃, **054305**, 1–19 (2012).
 36. Sosso, G. C., Caravati, S. & Bernasconi, M. Vibrational properties of crystalline Sb₂Te₃ from first principles. *J. Phys. Condens. Matter* **21**, (2009).
 37. Yao, J. D., Zheng, Z. Q., Shao, J. M. & Yang, G. W. Stable, highly-responsive and broadband photodetection based on large-area multilayered WS₂ films grown by pulsed-laser deposition. *Nanoscale* **7**, 14974–14981 (2015).
 38. Varghese, A. *et al.* Near-Direct Bandgap WSe₂/ReS₂ Type-II pn Heterojunction for Enhanced Ultrafast Photodetection and High-Performance Photovoltaics. *Nano Lett.* **20**, 1707–1717 (2020).
 39. Fan, Z. Q., Jiang, X. W., Chen, J. & Luo, J. W. Improving Performances of In-Plane Transition-Metal Dichalcogenide Schottky Barrier Field-Effect Transistors. *ACS Appl. Mater. Interfaces* **10**, 19271–19277 (2018).
 40. Chen, J. W. *et al.* A gate-free monolayer WSe₂ pn diode. *Nat. Commun.* **9**, (2018).
 41. Xiao, J., Zhang, Y., Chen, H., Xu, N. & Deng, S. Enhanced Performance of a Monolayer MoS₂/WSe₂ Heterojunction as a Photoelectrochemical Cathode. *Nano-Micro Lett.* **10**, (2018).
 42. Wang, L. *et al.* MoS₂/Si heterojunction with vertically standing layered structure for ultrafast, high-detectivity, self-driven visible-near infrared photodetectors. *Adv. Funct. Mater.* **25**, 2910–2919 (2015).
 43. Tian, R. *et al.* Chip-integrated van der Waals PN heterojunction photodetector with low dark current and high responsivity. *Light Sci. Appl.* **11**, (2022).
 44. Dai, M. *et al.* Ultrafast and Sensitive Self-Powered Photodetector Featuring Self-Limited Depletion Region and Fully Depleted Channel with van der Waals Contacts. *ACS Nano* **14**, 9098–9106 (2020).
 45. Huo, N. *et al.* Novel and enhanced optoelectronic performances of multilayer MoS₂-WS₂ heterostructure transistors. *Adv. Funct. Mater.* **24**, 7025–7031 (2014).
 46. Maiti, R. *et al.* Strain-Induced Spatially Resolved Charge Transport in 2H-MoTe₂. *ACS Appl. Electron. Mater.* **3**, 3781–3788 (2021).
 47. Heidari, E. *et al.* Integrated ultra-high-performance graphene optical modulator. *Nanophotonics* **0**, (2022).
 48. Dalir, H., Xia, Y., Wang, Y. & Zhang, X. Athermal Broadband Graphene Optical Modulator with 35 GHz Speed. *ACS Photonics* **3**, 1564–1568 (2016).
 49. Asghari, A. *et al.* Fast, accurate, point-of-care COVID-19 pandemic diagnosis enabled through advanced lab-on-chip optical biosensors: Opportunities and challenges. *Appl. Phys. Rev.* **8**, (2021).
 50. Fratalocchi, A. *et al.* Nano-optics gets practical Early-career researchers share their thoughts on how to make use of the ability to manipulate light at the nanoscale. *Nat. Nanotechnol.* **10**, 11–15 (2015).
 51. Sorger, V. J. Two-dimensional material nanowatt threshold lasing. *NPG Asia Mater.* **7**, 4057 (2015).
 52. Tahersima, M. H. & Sorger, V. J. Enhanced photon absorption in spiral nanostructured solar cells using

layered 2D materials. *Nanotechnology* **26**, (2015).